Circular photonic crystal resonators

Jacob Scheuer* and Amnon Yariv
Department of Applied Physics, 128-95 California Institute of Technology, Pasadena, California 91125, USA
(Received 12 April 2004; revised manuscript received 15 June 2004; published 9 September 2004)

We study analytically and numerically a new class of circular resonators based on a radial photonic crystal reflector. The Bragg confinement enables the realization of compact resonators exhibiting both large free spectral range and high *Q*-factor. The dependence of the resonator characteristics on the reflector architecture and dimensions is studied in detail. Good agreement is found between the analytical and the numerical results obtained by finite-difference time-domain simulations.

DOI: 10.1103/PhysRevE.70.036603 PACS number(s): 42.70.Qs, 42.82.−m, 42.79.Gn, 42.25.Bs

I. INTRODUCTION

Circular resonators are key ingredients in the realization of many basic components needed for advanced optical communication systems. During the last decade, numerous circular-resonator based applications such as filters [1], add/drop multiplexers [2], modulators [3], and delay lines [4] have been suggested and demonstrated. In addition, the applicability of circular resonators was shown to extend beyond telecommunication to the fields of sensing [5], spectroscopy, and standardization [6], as well as to basic research in QED, nonlinear optics, and other related fields [7,8].

For many of these applications, the circular resonator is required to exhibit low losses or, equivalently, a high quality factor (Q). In addition to high Q, it often desirable that the resonator has small dimensions or, equivalently, exhibits large free spectral range (FSR). Unfortunately, for conventional resonators, which utilize total internal reflection (TIR) as the radial confinement mechanism, these requirements are mutually contradicting. To exhibit large FSR, a circular resonator is required to have a short circumference and small bending radius. In these conditions, the efficiency of the TIR confinement mechanism is significantly impaired, leading to larger power dissipation and lower Q-factor [9].

For a given bending radius, the radial confinement and hence, the bending losses, can be improved by increasing the index contrast between the core and the cladding. On the other hand, this would decrease the FSR due to the increase in the effective index (propagation factor) of the electromagnetic field in the core. Since there is a limit to the refractive index value of available optically transparent materials, it is clear that the TIR mechanism inherently limits the ability to realize circular resonators with both low losses and large FSR.

Photonic crystal (PC) cavities have been extensively studied for high Q cavity applications (Q values up to 4.5×10^4 have been demonstrated) [10]. However, these resonators consist primarily of a defect (either point or line), which does not necessarily support a whispering-gallery-mode-like solution, or of hexagonal (noncircular) cavities incorporating 120° abrupt bends which tend to support localized bound states [11].

Recently, we have suggested utilizing Bragg reflection instead of TIR as the radial confinement mechanism in order to break the link between the FSR and the loss and facilitate low-loss, large FSR circular resonators [12]. This concept is illustrated in Fig. 1. A disk [Fig. 1(a)] or a circumferentially guiding defect [Fig. 1(b)] is located within a medium which consists of annular Bragg layers. The confinement of the modal field within the defect [Fig. 1(b)] or in the disk [Fig. 1(a)] is accomplished by Bragg reflection instead of TIR. Unlike conventional resonators, the reflectivity of the Bragg mirror can be increased simply by adding more layers. As a result, the radius of the defect (or the disk) can be reduced almost arbitrarily without the penalty of higher bending losses.

Disk and ring resonators based on distributed Bragg reflection were analyzed before for both laser and passive resonator applications, employing various techniques such as conformal mapping, coupled-mode approach, and field transfer matrices [13]. While circular symmetric structures, as shown in Fig. 1, can be modeled accurately by transfer matrix formalism [13], the analysis of noncircular symmetric structures (see Fig. 2) requires different tools. Recently, we developed a coupled-wave approach to design and analyze such structures [14].

In this paper, we study analytically and numerically the characteristics of disk resonators that utilize photonic crystal reflectors. The main advantage of this class of resonators, compared to the circular symmetric structures shown in Fig. 1, is that it is suited to a greater variety of realization concepts. Particularly, the fabrication of such structures is compatible with the suspended membrane concept which was proven to be very successful for PC defect cavities [10]. In addition, unlike the circular symmetric devices, the upper surface of the circular PC resonators is continuous and, therefore, supports the deposition of an electrical contact, thus enabling electrical pumping.

In Sec. II we briefly review the coupled-wave approach which is employed to design the resonators. In Sec. III we utilize this approach to design circular PC resonators and to study the impact of various photonic lattice designs on the resonators' spectral features, modal field profile, and Q-factor. In Sec. IV we study the impact of the reflector finiteness and in Sec. V we discuss the results and summarize.

*Electronic address: koby@caltech.edu

 ©2004 The American Physical Society

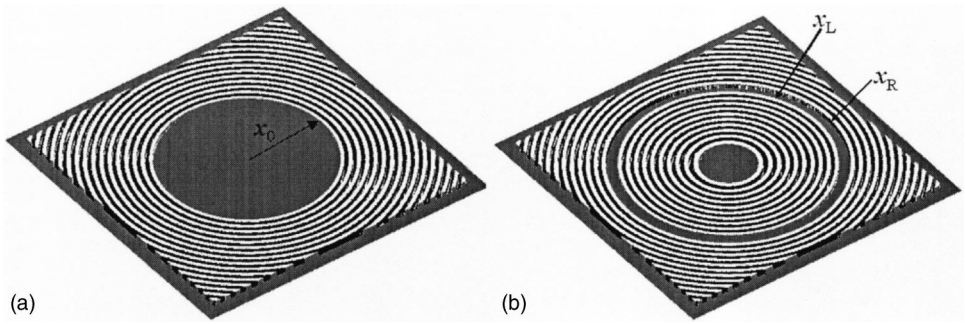

FIG. 1. An illustration of (a) a Bragg disk resonator; and (b) an annular defect mode (ring) resonator structure.

II. COUPLED-WAVE EQUATIONS

We consider a wave which propagates azimuthally in a structure as illustrated in Fig. 2; a disk of dielectric material which is surrounded by radial perturbation of the dielectric coefficient $\varepsilon(\rho)$. Assuming the electromagnetic field is well confined in the vertical dimension, the effective index approximation [15] can be used to reduce the 3D problem to an equivalent 2D problem. In the 2D geometry, the modal solutions can be separated into two independent polarizations: TE, consisting of E_z, H_ρ, and H_θ, and TM consisting of H_z, E_ρ, and E_θ, where ρ, θ, and z are, respectively, the radial, azimuthal, and axial coordinates [16]. All the electromagnetic field components can be expressed by the z component of either the electric (TE) or magnetic (TM) fields. In this paper, we focus on the TE polarization although the analysis of the TM polarization is similar.

We look for a modal solution of the Helmholtz equation in radial coordinates which is resonant in the structure shown in Fig. 2, with the following functional form:

$$E_z = E(\rho)\exp(im\theta), \tag{1}$$

where m is an integer. The radial part of the field satisfies the Bessel equation:

$$\rho^2\frac{d^2E}{d\rho^2} + \rho\frac{dE}{d\rho} + [k^2(\rho)\rho^2 - m^2]E = 0, \tag{2}$$

where $k(\rho)=k_0\varepsilon(\rho)$ is the wave number. We assume that the dielectric coefficient $\varepsilon(\rho)$ is given by $\varepsilon=n_0^2$ in the unperturbed area ($\rho<\rho_0$ in Fig. 2 and by $\varepsilon=n_0^2+\Delta\varepsilon(\rho)$ within the perturbed region. Introducing the normalized radius $x=k_0n_0\rho$ yields the dimensionless wave equation:

$$x^2E_{xx} + xE_x + [x^2 - m^2]E = 0, \quad x \leqslant x_0, \tag{3a}$$

$$x^2E_{xx} + xE_x + \left[x^2\left(1 + \frac{\Delta\varepsilon(x)}{n_0^2}\right) - m^2\right]E = 0, \quad x > x_0, \tag{3b}$$

where $x_0=k_0n_0\rho_0$ is the dimensionless radius of the disk. The solution of Eq. (3) in the disk region is given by a superposition of the mth order Hankel functions of the first and second kind. When the perturbation $\Delta\varepsilon(\rho)$ is small compared to n_0^2, the solution of Eq. (3) in the perturbed region can be written as slowly varying envelopes multiplying the Hankel functions:

$$E(x) = \begin{cases} \overline{A}H_m^{(1)}(x) + \overline{B}H_m^{(2)}(x), & x \leqslant x_0 \\ A(x)H_m^{(1)}(x) + B(x)H_m^{(2)}(x), & x > x_0. \end{cases} \tag{4}$$

Introducing Eq. (4) into Eq. (3b) and neglecting the second derivatives of $A(x)$ and $B(x)$ leads to [using Eq. (3a)]

$$\frac{dA}{dx}\left(2\frac{dH_m^{(1)}}{dx} + \frac{H_m^{(1)}}{x}\right) + \frac{dB}{dx}\left(2\frac{dH_m^{(2)}}{dx} + \frac{H_m^{(2)}}{x}\right) + \frac{\Delta\varepsilon}{n_0^2}(AH_m^{(1)} + BH_m^{(2)}) = 0, \tag{5}$$

where the specific x dependence of the amplitudes and the Hankel functions was dropped for clarity. In previous studies [13], the asymptotic approximation for the Hankel functions was used to derive a simplified equation, yielding complex exponentials in x as the required perturbation profile. Here we introduce the following approximation for large x: $H_m^{(1,2)}/x << dH_m^{(1,2)}/dx$ and $dH_m^{(1,2)}/dx \approx \pm iH_m^{(1,2)}$ [14]. Apparently, this approximation for the derivatives of the Hankel functions is more accurate than the derivative of the "conventional" asymptotic approximation (see [14] for more details).

Under these approximations, equation (5) can be rewritten as

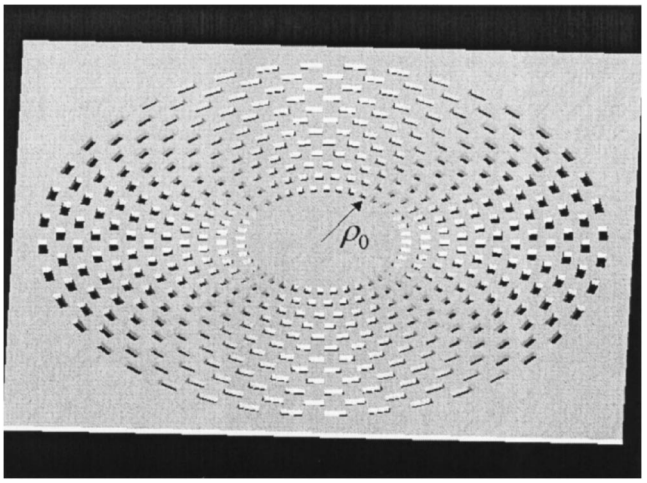

FIG. 2. Schematic index profile of a PC disk resonator. Gray: material; and black: air holes.

$$2i[H_m^{(1)}(x)A_x(x) - H_m^{(2)}(x)B_x(x)] + \frac{\Delta\varepsilon(x)}{n_0^2}[A(x)H_m^{(1)}(x) + B(x)H_m^{(2)}(x)] = 0. \quad (6)$$

It should be noted that $H_m^{(1)}$ and $H_m^{(2)}$ represent incoming and outgoing cylindrical waves. In view of Eq. (6) it is clear that the perturbation $\Delta\varepsilon$, which is required to efficiently couple power between the incoming and outgoing waves, should have the following form:

$$\Delta\varepsilon(x) = \alpha\frac{H_m^{(2)}(x)}{H_m^{(1)}(x)} + \alpha^*\frac{H_m^{(1)}(x)}{H_m^{(2)}(x)}, \quad (7)$$

where a is a complex amplitude of the perturbation. Introducing Eq. (7) into Eq. (6) and keeping only the first order in $H_m^{(1)}$ and $H_m^{(2)}$ (as in the derivation of Cartesian coupled mode theory) yields a set of coupled equations for the wave amplitudes A and B:

$$2i\frac{dA(x)}{dx} + \frac{\alpha^*}{n_0^2}B(x) = 0,$$

$$-2i\frac{dB(x)}{dx} + \frac{\alpha}{n_0^2}A(x) = 0. \quad (8)$$

Since $H_m^{(1)}$ and $H_m^{(2)}$ are complex conjugates of each other, the ratio between them is twice the phase φ of the numerator and Eq. (7) can be written as

$$\Delta\varepsilon = 2|\alpha|\cos\{2\varphi(H_m^{(1)}) - \varphi_\alpha\}, \quad (9)$$

where φ_α is the phase of α. It is worth noting that the coupled amplitude equations (8) and the required perturbation profile (9) exhibit fundamental resemblance to the Cartesian case [16]. In both cases, the perturbation is determined by the phase of the eigenmodes of the wave equation in the appropriate coordinates (plane wave for the Cartesian case and Hankel functions for the cylindrical case).

The equations set (8), which describe the evolution of the amplitudes of the cylindrical waves in ρ, can be readily solved:

$$A(x) = A_1\exp(kx) + A_2\exp(-kx),$$

$$B(x) = -i\frac{k}{k^*}[A_1\exp(kx) - A_2\exp(-kx)], \quad (10)$$

where $k=\alpha/2n_0^2$ is the coupling coefficient between the outgoing and incoming waves. Knowing the perturbation profile needed to attain radial confinement (9) and the modal field profile (10), it is possible to design and analyze a circular distributed feedback resonator.

III. CIRCULAR PHOTONIC CRYSTAL RESONATORS

In this section, we employ the results of the previous section to design and analyze a disk resonator which is based on a circular PC reflector. The modal field characteristics are verified and studied further by finite difference time domain (FDTD) simulations.

A schematic of a circular PC resonator structure is shown in Fig. 2. Since we attempt to design a resonator, we need to know the required resonance wavelength λ and the modal field azimuthal number m. Knowing that the required perturbation profile is given by Eq. (9), the parameters left to be determined are α and the disk radius x_0.

Inside the disk ($x<x_0$), the modal field is given by Eq. (4). For the field to be finite at $x=0$ it is required that the amplitudes of the incoming and outgoing waves are equal, i.e., $\overline{A}=\overline{B}$. As a result, the field at $x<x_0$ is given by $J_m(x)$ where J_m is the mth order Bessel function of the first kind. In the grating region ($x>x_0$) the field profile is given by Eq. (10). For simplicity, we assume that the gratings extend to very large radius so that the exponentially increasing term in Eq. (10) vanishes, i.e., $A_1=0$. At the interface between the disk and the grating ($x=x_0$), both the field and its derivative must be continuous (for TE polarization). The phase of the coupling coefficient $k=|k|\exp(i\varphi_k)$ (or α) can be, in principal, selected arbitrarily (as for Cartesian Bragg reflectors), it merely introduces a spatial shift of the gratings (9). However, this phase affects the required disk radius, x_0, which satisfies the boundary conditions. For the specific case of $\varphi_k=\pi/2$, the characteristic equation for x_0 is simple: $J_m(x_0)=0$. In this case, the required perturbation and field profiles are given by

$$\Delta\varepsilon(x) = \begin{cases} 0, & x < x_0 \\ -2|\alpha|\sin[2\varphi(H_m^{(1)}(x))] & x \geqslant x_0, \end{cases} \quad (11a)$$

$$E(x) = \begin{cases} J_m(x), & x < x_0 \\ J_m(x)\exp[-|k|(x-x_0)], & x \geqslant x_0. \end{cases} \quad (11b)$$

Equation (11) yields both the pertinent perturbation term and the field profile. In order to radially confine the mode, the perturbation profile must include a term with the functional form of Eq. (11a). To realize a PC reflector, we suggest the following index profile:

$$\varepsilon(x,\theta) = \begin{cases} n_0^2 - (n_0^2 - n_p^2)\Im[2\varphi(H_m^{(1)}(x)),\alpha_1]\Im[l\theta,\alpha_2], & x > x_0 \\ n_0^2, & x \leqslant x_0, \end{cases}$$

$$\Im(y,\alpha) = \begin{cases} 0, & \sin(y) < \alpha \\ 1, & \sin(y) \geqslant \alpha, \end{cases} \quad (12)$$

where $-1<\alpha_1,\alpha_2<1$, n_0 is the material index of refraction and l is the azimuthal number of the index profile. The structure consists of a dielectric material of refractive index n_0 perforated by holes with refractive index n_p.

This index profile is the radial equivalent of a rectangular PC with rectangular holes. The perforation function $\Im(y,\alpha)$ can be interpreted as a generalized rectifier of $\sin(y)$, generating square "pulses" only where $\sin(y)>\alpha$. The larger the value of α, the narrower the "pulses." The index profile (12) includes two $\Im$ functions: the first generates annular slits centered at the maxima of $\sin\{2\varphi[H_m^{(1)}(x)]\}$ with widths that are determined by α_1. The second $\Im$ function modulates these slits as a function of the angle θ with angular frequency l and "duty-cycle" determined by α_2.

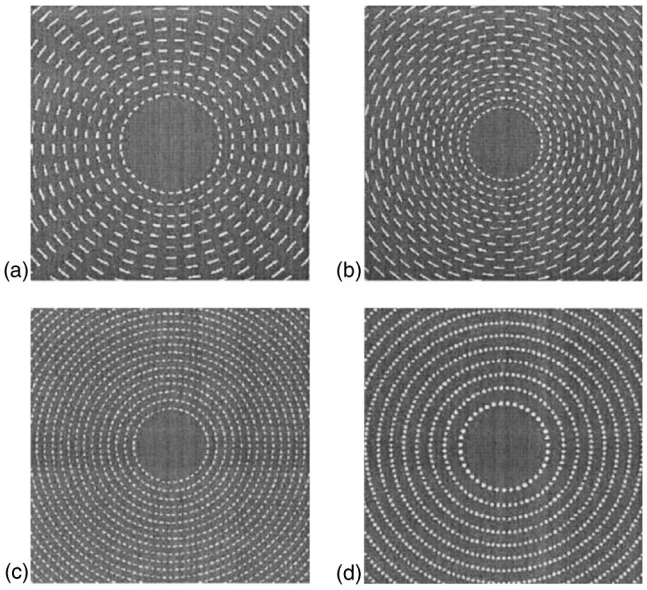

FIG. 3. The different reflector types: (a) "rectangular" lattice, (b) "triangular" lattice, (c) "varying-l" lattice with rectangular holes, and (d) "varying–l" lattice with circular holes.

For $n_p=1$ (air holes), the Fourier expansion of the perforation function $\Im(y,\alpha)$ is given by

$$\Im(y,\alpha) = \cos^{-1}(\alpha)/\pi - \sum_{m=1}^{\infty} \frac{(-1)^m - 1}{m\pi} \cos[m \sin^{-1}(\alpha)]\sin(my) - \sum_{m=1}^{\infty} \frac{(-1)^m + 1}{m\pi} \sin[m \sin^{-1}(\alpha)]\cos(my). \quad (13)$$

The term which is responsible for the radial confinement of the modal field is the first order in the radial expansion and zero order in the azimuthal expansion, which is given by

$$\Delta\varepsilon_{1,0} = -2(n_0^2 - 1)\cos[\sin^{-1}(\alpha_1)]\cos^{-1}(\alpha_2)/\pi^2. \quad (14)$$

The fact that $\Delta\varepsilon_{1,0}$ is independent of the azimuthal number of the perturbation, l, indicates that the azimuthal details of the index profile are of less significance. The azimuthal modulation is averaged over the device circumference and its only influence on the coupling coefficient is through the "filling factor" $\cos^{-1}(\alpha_2)$. A similar conclusion was also deduced for microstructured fibers [17]. It should be clear, however, that this result stems directly from neglecting all the terms in Eq. (12) except $\Delta\varepsilon_{1,0}$, which is accurate only if $l \gg m$. Nevertheless, in this limit the conclusion holds and the azimuthal dependence of Eq. (12) can be modified without deteriorating the performances of the device.

In the remainder of this section, we verify the results of the coupled-wave analysis using FDTD simulations. We study the spectral characteristics and Q-factor of circular PC resonators that employ reflectors of different geometries. The PC-reflector types are illustrated in Fig. 3. Figure 3(a) depicts a "rectangular lattice" consisting of the perturbation profile (12). Figure 3(b) depicts a "triangular"-type lattice PC reflector, in which every other "necklace" of holes is rotated by π/l (l is the azimuthal periodicity of the perturbation). The dielectric profile of this lattice for $x > x_0$ is given by

$$\varepsilon_{\text{triangular}}(x,\theta) = n_0^2 - (n_0^2 - n_p^2)\{\Im(2\varphi[H_m^{(1)}(x)],\alpha_1) \times \Im(\varphi[H_m^{(1)}(x)],0)\Im(l\theta,\alpha_2) + \Im(2\varphi[H_m^{(1)}(x)],\alpha_1)[1 - \Im(\varphi[H_m^{(1)}(x)],0)] \times \Im[l\theta + \pi,\alpha_2]\}. \quad (15)$$

The perturbation in Eq. (15) consists of two terms where one of them generates the rotated necklaces of holes and the other generates the nonrotated necklaces. An additional $\Im$ function was used to distinguish between the two sets of holes. The leading term of the perturbation profile can be calculated by substituting Eq. (13) into Eq. (15) and keeping only the terms with first order in ρ and zero order in θ. Not surprisingly, the outcome of this calculation is identical to the "rectangular" lattice case (14).

Figure 3(c) depicts a reflector which does not consist of a single azimuthal modulation frequency. This type of reflector was constructed with an attempt to keep the hole shapes as close as possible to an ideal square. As a result, the number of holes per "necklace" increases for larger radii. We designate this type of reflector as a "varying–l" lattice. This type of reflector does not have an equivalent Cartesian PC because it does not form a genuine crystal. Nevertheless, in the small perturbation regime we expect the characteristics of such a resonator to be similar to those of the resonators shown in Figs. 3(a) and 3(b).

In the resonator depicted in Fig. 3(d), the concept described in the previous paragraph was extended further. It is reasonable to assume that if the holes perforating the medium are small, their actual shape is of less significance and that the important factor is their area. The reflector in Fig. 3(d) was constructed by replacing each hole in Fig. 3(c) with a circular hole which has the same area. Again, we can expect the resonator characteristics to remain unaffected.

Figure 4 compares the numerically calculated radial mode profiles of various resonator types which have the same α_1 and α_2 parameters and the analytically calculated profile (11b). The wavelength is 1.52 μm and the parameters of the structures are defined in the figure caption. The numerical solutions indicate that, as expected, the mode profiles of the different structures are practically identical. In addition, the good agreement with the approximated analytical solution is clear, even though the index contrast in the reflector region is relatively high.

Figure 5 depicts the resonance frequencies calculated by two-dimensional FDTD for several PC reflector structures (α_1 and α_2 are the same for all structures). The spatial resolution was 0.01 μm. The resonances were calculated by exciting the structure with a very short pulse (20 fs) and letting it circulate in the resonator for a long period while monitoring the field amplitude at the peak of the mode. Taking the Fourier transform of the field yields the spectral response of the resonator. The spectral responses of all the structures are almost identical, with resonaces at $l=1.52$ μm for $m=8$ (the

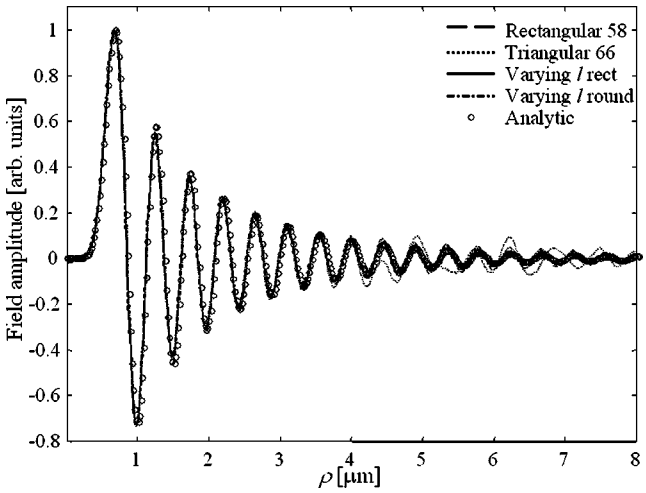

FIG. 4. Comparison between the modal field profiles of the different resonator structures: "rectangular" lattice with $l=58$ (dashed), "triangular" lattice with $l=66$ (dotted), "varying-l" lattice with rectangular holes (solid), "varying-l" lattice with circular holes (dash-dot), and analytical solution (circles). The other parameters of the structure are $n_0=3.5$, $m=8$, $\alpha_1=0.9$, and $\alpha_2=0$.

target mode) and at 1.455 μm for $m=9$. The inset of Fig. 5 shows the modal field profiles at the resonance frequencies and the corresponding field profiles, which are also identical for all structures. It is evident that the field profile of $m=8$ is more confined in the resonator than the field profile of $m=9$. This is because the radial part of the gratings is designed for $m=8$ and, as a result, the $m=9$ mode has a smaller decay coefficient in the gratings. This is in contrast to conventional (TIR based) disk resonators for which higher m numbers are generally associated with more grazing incidence angles of the field at the interface. These modes are confined more strongly in the disk and, therefore, experience lower bending losses.

According to Eq. (14), the modal field profile of the resonator is independent of the azimuthal frequency of the perturbation, l. Figure 4, which depicts the field profile for various structures, indicates that this is indeed correct. Moreover, as shown in Fig. 5, the spectral response (i.e., the resonance wavelengths) of the resonators is almost independent of the lattice type and the azimuthal perforation frequency. It is, therefore, interesting to examine whether the quality factor is also independent of the reflector architecture. Figure 6 shows the dependence of the ringdown time constant (and, hence, the Q) on the azimuthal perforation frequency l. The ringdown time constant is a measure for the photon lifetime in the cavity and it is related to the Q according to

$$Q = w_0 \tau_0, \tag{16}$$

where w_0 is the resonance (angular) frequency of the resonator.

It seems that the general trend is that higher Q factors are attained for larger values of l for both the triangular and the rectangular lattices. However, there is a clear decrease in the Q for $l=56$, most probably due to grating assisted phase matching to a radiating mode. The simulations also indicate that a rectangular lattice reflector exhibits lower losses compared to a triangular lattice reflector with the same angular perturbation frequency. Nevertheless, as seen in Fig. 6, a

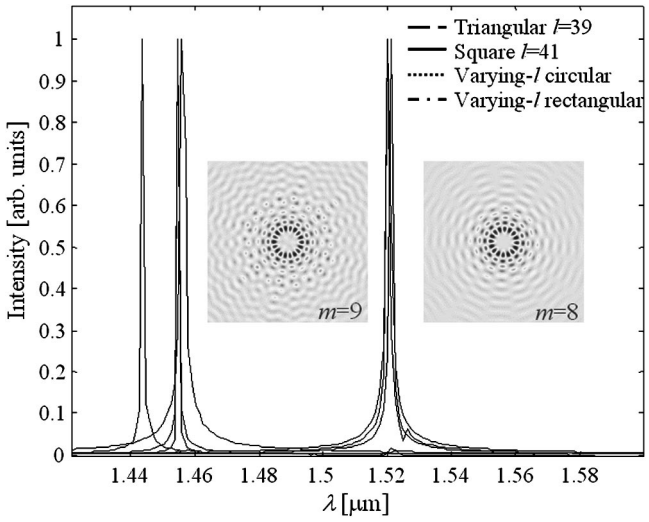

FIG. 5. Resonance frequencies of the various structures: "triangular" lattice with $l=39$ (dashed), "rectangular" lattice with $l=41$ (solid), "varying-l" lattice with circular holes (dotted), and "varying-l" lattice with rectangular holes (dash-dot). The inset shows the corresponding field profiles.

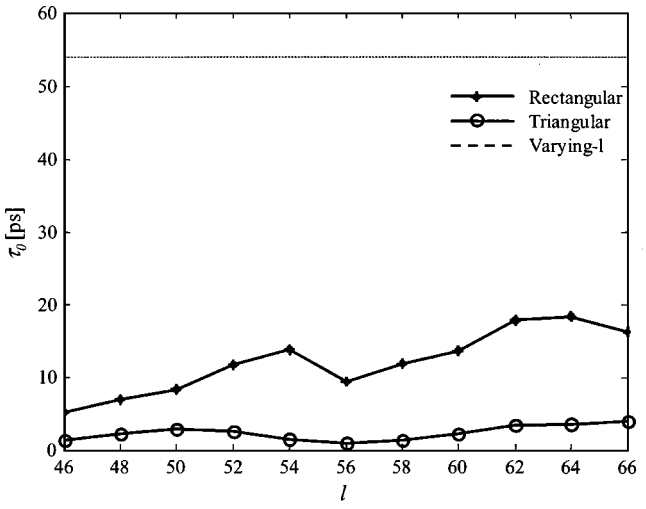

FIG. 6. The cavity ringdown time constant as function of the azimuthal perturbation frequency l: and "rectangular" lattice (solid) and "triangular" lattice (dashed). The dash-dot line indicates the ringdown time constant of the "varying-l" lattice with rectangular holes.

reflector consisting of higher angular perturbation frequency for larger radii ("varying-l") is significantly superior (from the quality factor point of view) to a reflector with constant angular perturbation frequency. This result can be understood as stemming from the dependence of the Q on l. At larger radii, the angular frequency of the "varying-l" reflector increases and, as a result, the reflectivity of the gratings is improved.

The fact that the coupled-wave approach does not predict different characteristics for the various lattice types and values of l is not surprising. The information on the azimuthal perforation profile is lost in the selection of $\Delta\varepsilon_{1,0}$ as the perturbation term. This term is influenced by the azimuthal properties of the lattice only through the mean azimuthal "filling factor" which is independent of l. To account for the impact of the higher order azimuthal terms, a cylindrical equivalent of the more rigorous coupled-wave analysis has to be developed [18]. This is, however, beyond the scope of this paper.

The analysis given here is two-dimensional and, therefore, does not account for out-of-plain radiation losses. It has been recently shown that, under certain circumstances, the out-of-plain losses could be the dominant mechanism which limits the attainable Q of a PC cavity [19]. These vertical radiation losses stem from low spatial frequency components of the modal field profile which do not satisfy the vertical TIR condition. However, a significant part of these losses can by canceled by careful optimization of the index profile, especially if the modal field and, correspondingly, the index profile are modified to have a more radial symmetry. Ryu *et al.* showed that it is possible to improve the vertical Q of a PC $H2$ cavity by a factor of 100 simply by rearranging the 12 nearest-neighbor holes more symmetrically and decreasing their size [19]. The structure of a circular PC resonator and its mode profile already possess the desired radial symmetry and are expected to exhibit low vertical radiation losses.

IV. FINITE GRATINGS

The field profile shown in Eq. (11b) was calculated under the assumption of infinitely long gratings. Under this assumption, the reflection coefficient of the Bragg mirror is unity and the electromagnetic field propagates in the resonator without loss (assuming there is no material absorption). However, in any practical device the gratings' length is finite and, therefore, part of the energy in the resonator "leaks" or radiates to the device surroundings.

The coupled-wave equations (8) and their solution (10) can be used to evaluate the power leakage due to the finiteness of the gratings. Figure 7 shows a radial cross section of the resonator structure and the z component of the electric field in the three distinct regions of the device: the inner disk, the Bragg reflector, and the external surroundings. To account for the power leakage, we assume that the Bragg mirror has a reflection coefficient $|r|<1$ and a transmission coefficient t. The electric field in the different regions is given by:

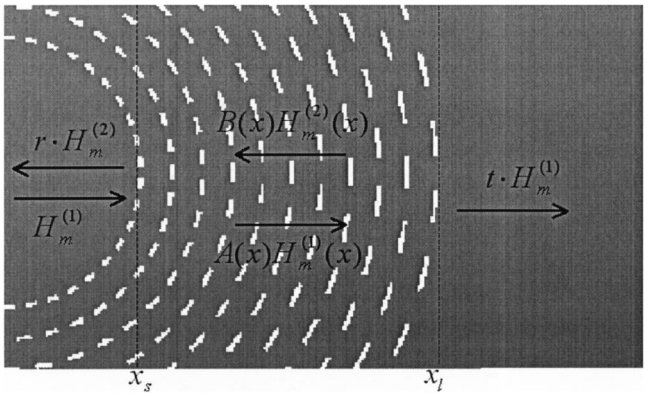

FIG. 7. Schematic cross section of the resonator structure, illustrating the amplitudes of the inward and outward propagating field components in each relevant region.

$$E_z = \begin{cases} H_m^{(1)}(x) + rH_m^{(2)}(x), & x < x_0 \\ A(x)H_m^{(1)}(x) + B(x)H_m^{(2)}(x), & x_0 \leqslant x \leqslant x_l \\ tH_m^{(1)}(x), & x > x_l, \end{cases} \quad (17)$$

where x_l is the normalized external radius of the gratings and $A(x)$ and $B(x)$ are given by Eq. (10). The amplitude of the field in one of the regions can be selected arbitrarily. In Eq. (17), the amplitude of the outgoing field in the inner disk was selected to be 1. Requiring the boundary conditions at x_0 and x_l (for TE, continuity of the field and its derivative) yields expressions for the reflection and transmission of the Bragg mirror, which under the assumptions of small coupling and the fact that $J_m(x_0)=0$, are given by

$$r = \tanh[|k|(x_l - x_0)],$$

$$t = 1/\cosh[|k|(x_l - x_0)], \quad (18)$$

where r and t satisfy the conservation of power $r^2+t^2=1$.

The reflection coefficient r indicates the fraction of the field amplitude which remains in the cavity after each "bounce" of the field from the Bragg mirror. The number of "bounces" in a single roundtrip is equal to the azimuthal number of the mode, m. Therefore the power loss in the cavity per revolution due to the finiteness of the structure in given by

$$L = 1 - r^{2m} = 1 - \tanh^{2m}[|k|(x_l - x_0)]. \quad (19)$$

The loss per revolution (19) is related to the cavity ringdown time constant through the energy velocity of the modal field in the resonator [20]. The roundtrip time is given by the ratio between the total energy stored in the resonator and the power flow through a radial cross section in the structure:

$$\tau_{\mathrm{RT}} = \frac{\frac{1}{4}\int\int(\varepsilon_0 n^2|E|^2 + \mu_0|E|^2)\rho d\rho d\theta}{\frac{1}{2}\int_{\infty}^{0}\mathrm{Re}(EH^*)d\rho}. \quad (20)$$

The power loss per roundtrip (19) corresponds to the decay in the field intensity within a single roundtrip time, equal to

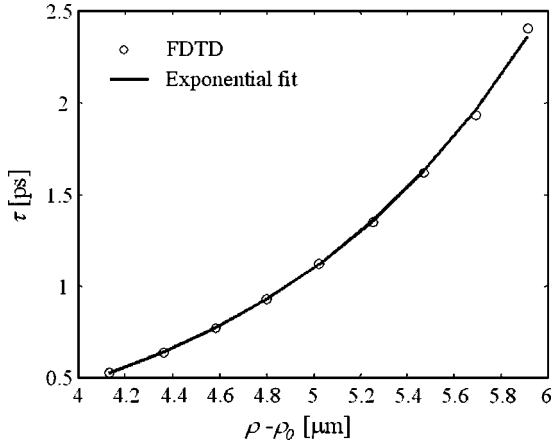

FIG. 8. FDTD calculated cavity ringdown constant as a function of the grating "length," $x_l - x_0$, and an exponential fit for a "varying-l" type resonator with rectangular holes.

$\exp(-\tau_{\mathrm{RT}}/\tau_0)$, where τ_0 is the cavity ringdown time constant. Equating the two quantities yields an expression for τ_0:

$$\tau_0 = -\frac{\tau_{\mathrm{RT}}}{2m\ \ln\{\tanh[|k|(x_l - x_0)]\}} \underset{k \ll 1}{\approx} \frac{\tau_{\mathrm{RT}}}{4m} \exp[2|k|(x_l - x_0)]. \tag{21}$$

Figure 8 depicts the cavity ringdown constant as a function of the reflector "length," $x_l - x_0$ for a "varying-l" type resonator (see Fig. 3) calculated by FDTD simulations and a fit based on Eq. (21). The parameters of the resonator are the same as in Fig. 4. It is clear that the ringdown time constant is indeed an exponential function of the grating length. The coupling coefficient k extracted from Fig. 8 is approximately 0.03 which is quite close to the predicted value of 0.032 given by Eq. (14).

Figure 9 depicts the field calculated by an FDTD simulation of a "varying-l" type resonator where the reflector is finite with an external radius of 5.3μm. The existence of the radiating field at radii larger than the 5.3μm is clearly visible. It should be emphasized that adding layers to the reflector does not change the FSR or even the resonance frequencies of the device.

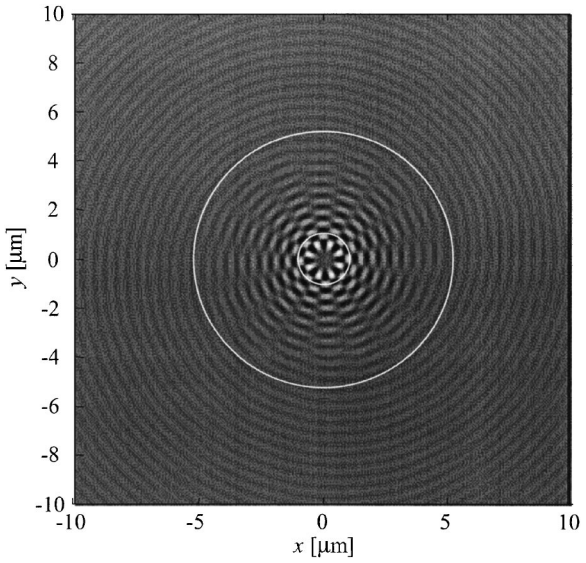

FIG. 9. Field profile of a "varying-l" type resonator with a 5.3μm "long" reflector. The white lines indicate the reflector region.

V. DISCUSSION AND SUMMARY

We have studied, analytically and numerically, the characteristics of circular resonators that are based on a PC reflector, using the FDTD algorithm and a coupled-wave approach. In the limit of small perturbations, the actual angular profile of the reflector is of minor significance for many of the resonator characteristics, with the important factor being the average "filling factor" of the perforation. Several lattice and "quasi-lattice" types were suggested and studied, all exhibiting similar spectral responses and mode profiles even beyond the small perturbations limit. The effect of the reflector finiteness on the cavity ringdown time constant was also studied, showing that this time constant (and hence the Q-factor) is exponentially increasing with the reflector length. The exponential growth factor equals twice the coupling coefficient between the incoming and outgoing waves. Good agreement was found between the analytically calculated field profile and ringdown time constant, and the numerically obtained results, even for relatively high index contrasts.

While the modal field profiles and the spectral response of the resonator seem to be independent of the azimuthal properties of the perturbation, the Q-factor increases as a function of l, even when $l \gg m$. In addition, rectangular lattice reflectors exhibit lower losses compared to the corresponding triangular lattice reflectors. However, the "varying-l" type resonator exhibits a much higher Q (by almost a factor of 10) compared to the fixed l resonators. At first glance, this result seems counterintuitive because the electromagnetic wave is not expected to be influenced by features that are much smaller than the field effective wavelength. Nevertheless, the coupled-wave approach presented here accounts only for the first order terms in the perturbation. Since the structures analyzed here exhibit high index contrast (3.5 vs 1) it is likely that higher order terms have non-negligible impact.

The bending losses of the PC circular resonator were shown to be decoupled from the FSR and even from the actual resonance wavelength of the cavity. Lower losses and higher Q can be attained simply by adding more layers to the reflector (see Fig. 6). The decoupling of the resonator FSR and resonance frequencies from the bending losses is a significant advantage of the circular PC resonators which paves the way to the realization of compact devices exhibiting both high Q and large FSR.

ACKNOWLEDGMENTS

The authors would like to thank George T. Paloczi, William M. J. Green, Joyce K. S. Poon, and George Ouyang for helpful discussions and comments. This work was supported by the National Science Foundation.

[1] C. K. Madsen and J. H. Zhao, *Optical Filter Design and Analysis: A Signal Processing Approach* (Wiley-Interscience, New York, 1999).
[2] B. E. Little, Opt. Lett. **23**, 1570 (1998); A. Melloni, R. Costa, P. Monguzzi, and M. Martinelli, *ibid.* **28**, 1567 (2003).
[3] A. Yariv, IEEE Photonics Technol. Lett. **14**, 483 (2002).
[4] J. E. Heebner and R. W. Boyd, J. Mod. Opt. **49**, 2629 (2002); A. Melloni, F. Morichetti, and M. Martinelli, Opt. Quantum Electron. **35**, 365 (2003); J. K. S. Poon, J. Scheuer, S. Mookherjea, G. T. Paloczi, Y. Huang, and A. Yariv, Opt. Express **12**, 90 (2004).
[5] C. Y. Chao and L. J. Guo, Appl. Phys. Lett. **83**, 1527 (2003).
[6] A. B. Matsko, L. Maleki, A. A. Savchenkov, and V. S. Ilchenko, J. Mod. Opt. **50**, 2523 (2003).
[7] See, for example, K. J. Vahala, Nature (London) **424**, 839 (2003), and references therein.
[8] J. Vučković, M. Lončar, H. Mabuchi, and A. Scherer, Phys. Rev. E **65**, 016608 (2001).
[9] E. A. J. Marcatili, AT&T Tech. J. **48**, 2103 (1969).
[10] Y. Akahane, T. Asano, B. S. Song, and S. Noda, Nature (London) **425**, 944 (2003); O. Painter, R. K. Lee, A. Scherer, A. Yariv, J. D. O'Brien, P. D. Dapkus, and I. Kim, Science **284**, 1819 (1999); C. J. M. Smith, H. Benisty, D. Labilloy, U. Oesterle, R. Houdré, T. F. Krauss, R. M. De La Rue, and C. Weisbuch, Electron. Lett. **35**, 228 (1999); S. H. Kim and Y. H. Lee, IEEE J. Quantum Electron. **39**, 1081 (2003); H. Benisty, C. Weisbuch, D. Labilloy, M. Rattier, C. J. M. Smith, T. F. Krauss, R. M. De La Rue, R. Houdré, U. Oesterle, C. Jouanin, and D. Cassagne, J. Lightwave Technol. **17**, 2063 (1999); R. K. Lee, O. J. Painter, B. D'Urso, A. Scherer, and A. Yariv, Appl. Phys. Lett. **74**, 1522 (1999); A. Scherer, O. Painter, B. D'Urso, R. Lee, and A. Yariv, J. Vac. Sci. Technol. B **16**, 3906 (1998); S. Kim, H. Ryu, H. Park, G. Kim, Y. Choi, Y. Lee, and J. Kim, Appl. Phys. Lett. **81**, 2499 (2002).
[11] A. Mekis, S. Fan, and J. D. Joannopoulos, Phys. Rev. B **58**, 4809 (1998).
[12] J. Scheuer and A. Yariv, J. Opt. Soc. Am. B **20**, 2285 (2003).
[13] J. Scheuer and A. Yariv, Opt. Lett. **28**, 1528 (2003); J. Scheuer, W. Green, G. DeRose, and A. Yariv, Proceedings of the SPIE - Photonics West 2004 Conference on Laser Resonators and Beam Control VII, San-Jose, CA., paper 5333-35; M. Toda, IEEE J. Quantum Electron. **26**, 473 (1990); X. H. Zheng and S. Lacroix, J. Lightwave Technol. **8**, 1509 (1990); T. Erdogan and D. G. Hall J. Appl. Phys. **68**, 1435 (1990); T. Erdogan and D. G. Hall, IEEE J. Quantum Electron. **28**, 612 (1992); M. A. Kaliteevski, R. A. Abram, V. V. Nikolaev, and G. S. Sokolovski, J. Mod. Opt. **46**, 875 (1999); C. Wu, M. Svilans, M. Fallahi, T. Makino, J. Glinski, C. Maritan, and C. Blaauw, Electron. Lett. **27**, 1819 (1991); D. Labilloy, H. Benisty, C. Weisbuch, T. F. Krauss, C. J. M. Smith, R. Houdré, and U. Oesterle, Appl. Phys. Lett. **73**, 1314 (1998); A. Shaw, B. Roycroft, J. Hegarty, D. Labilloy, H. Benisty, C. Weisbuch, T. F. Krauss, C. J. M. Smith, R. Stanely, R. Houdré, and U. Oesterle, *ibid.* **75**, 3051 (1999); D. Ochoa, R. Houdré, M. Ilegems, H. Benisty, T. F. Krauss, and C. J. M. Smith, Phys. Rev. B **61**, 4806 (2000).
[14] J. Scheuer and A. Yariv, IEEE J. Quantum Electron. **39**, 1555 (2003).
[15] D. Marcuse, *Theory of Dielectric Optical Waveguides*, edited by P. F. Liao and P. L. Kelley (Academic, Boston, 1972).
[16] See, for example, A. Yariv, *Optical Electronics in Modern Communications*, 5th ed. (Oxford University Press, New York, 1997).
[17] S. E. Golowich and M. I. Weinstein, J. Opt. Soc. Am. B **20**, 633 (2003).
[18] G. V. Morozov, D. W. L. Sprung, and J. Martorell, Phys. Rev. E **69**, 016612 (2004); M. G. Moharam, E. B. Grann, and D. A. Pommet, J. Opt. Soc. Am. A **12**, 1068 (1995); B. P. Kirsanov and M. V. Krongauz, *ibid.* **13**, 2423 (1996); T. Iizuka and C. M. de Sterke, Phys. Rev. E **61**, 4491 (2000).
[19] J. Vučković, M. Lončar, H. Mabuchi, and A. Scherer, IEEE J. Quantum Electron. **38**, 850 (2002); K. Srinivasan and O. Painter, Opt. Express **10**, 670 (2002); H. Y. Ryu, M. Notomi, and Y. H. Lee, Appl. Phys. Lett. **83**, 4294 (2003); H. Y. Ryu, M. Notomi, G. H. Kin, and Y. H. Lee, Opt. Express **12**, 1708 (2004).
[20] A. Yariv and P. Yeh, *Optical Waves in Crystals* (J. Wiley, New York, 1984).